ACS MATERIALS Au
AN OPEN ACCESS JOURNAL OF THE AMERICAN CHEMICAL SOCIETY

pubs.acs.org/materialsau
Article

Utilization of Electrocoagulated Sewage as a Photoelectrocatalyst for Water Splitting

Lalita Sharma, Jyoti Rohilla, Pravin P. Ingole, and Aditi Halder*

Cite This: ACS Mater. Au 2024, 4, 459−467
Read Online

ACCESS | Metrics & More | Article Recommendations | Supporting Information

ABSTRACT: Electrocoagulation (EC) as a wastewater treatment process for the removal of pollutants has been demonstrated in numerous studies. However, proper management of solid waste generated after EC treatment is essential to minimize its environmental impact. Hence, more emphasis needs to be paid towards unused solid waste after EC treatment. The present study investigates the possibilities of utilizing waste released after the EC process as an electrocatalyst in the presence of sunlight. In this study, the sludge produced after domestic wastewater treatment by the EC process is collected and tested for water oxidation reaction under AM 1.5 illumination of simulated solar light. The sludge produced after EC treatment was characterized meticulously and confirmed to be the magnetite phase of iron oxide, which is used as a photoanode for photoelectrochemical (PEC) water splitting. The chemical composition of sludge is majorly dependent on the treatment time, which plays a crucial role in deciding the metal ions present in the sludge. After 30 min, which is the optimized time for EC treatment, sludge was studied as an efficient photoanode material. The band gap illumination of sludge (iron oxide) as working electrodes results in anodic current; the photocurrent appears at a bias of ca. 390 mV with respect to the flat-band potential. The PEC activity of waste is treatment-time dependent and decreases after reaching an optimal time of 30 min. A photocurrent density of 4.6×10^{-6} A cm^{-2} was found at the potential of 1.23 V (vs RHE) for sludge collected after 30 min of treatment time. It indicates that the sludge-derived photoanode has the potential to be an efficient component in PEC systems, contributing to the overall efficiency of water-splitting processes. Our experimental results show a new pathway of a "waste to energy" approach that aligns with the principles of circular economy and sustainable resource management.

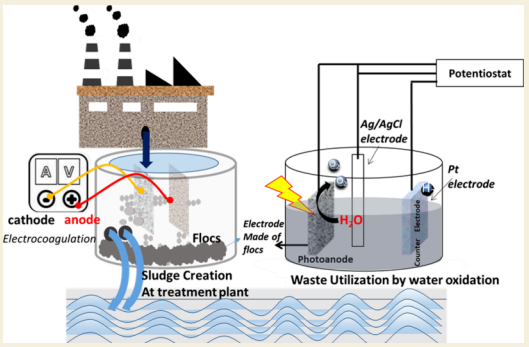

KEYWORDS: *waste water treatment, electrocoagulation, sludge recovery, photoelectrocatalyst, water splitting*

1. INTRODUCTION

Waste is defined as an unwanted product in the environment released from the manufacturing process from industry, agriculture, and household activity. Waste causes many environmental hazards that affect the survival of living species (humans and animals) on earth. Thus, sustainable waste management is a crucial and necessary action to be adopted, where the reuse and recycling of waste into value-added products are essential mandates. Wastewater treatment by using the electrocoagulation (EC) technique is a well-adopted and widely used technique, where iron (Fe) is used at the anode and aluminum (Al) is used at the cathode, respectively.[1] However, the disposal of the waste produced by the EC process creates a hazardous threat due to the higher concentration of Al present in it.[2] Environment and energy problems are the two major issues that human beings have been facing. It will be worth investigating how to utilize these waste-derived materials as environmentally friendly, low-cost, value-added products for energy generation.

Solar energy is the largest source of renewable energy (~1.2×10^{14} kJ) received by the earth's crust every second.[3] So, the integration of solar light with electrochemical water splitting is of considerable interest. Solar-assisted photoelectrochemical (PEC) water splitting is considered to be an effective strategy for zero-carbon emission energy production.[4] It involves the hydrogen (H_2) production at the cathode and oxygen (O_2) evolution reaction at the anode, respectively, in an aqueous electrolyte. In this approach, electrocatalysts are demanded to minimize the overall overpotential of the water-splitting reactions.[5] For the advancement of this technology, developing efficient and inexpensive catalysts has been one of the hot research topics in the field of solar water splitting. In the case of H_2 evolution (water reduction), transition metal alloys, sulfides, and phosphides are promising candidates to meet the criteria of high efficiency and low cost.[6,7] In the case of water

Received: February 2, 2024
Revised: February 18, 2024
Accepted: February 21, 2024
Published: March 1, 2024

oxidation reaction, most active earth-abundant materials are transition metal hydroxides or oxides[6,8,9] such as WO_3,[10] Fe_2O_3,[11] and $BiVO_4$[12] and other metal oxide based semiconductor photoanode materials utilized in PEC water splitting. The water oxidation step is substantially 5 orders slower than the water reduction step.[13] Many efforts have been undertaken to search for highly active and stable photoanode materials. However, they require many complex reactions and expensive chemicals. It is worth investigating whether waste derived from other technologies can be utilized for the production of these electroactive materials.

In this work, we utilized waste (solid sludge) produced by the EC technique for energy generation. EC is a multistep process used for the treatment of wastewater being run by an external supply of electric current.[14,15] In the EC technique, in situ coagulants are produced because of the redox reactions that happen at the surface of electrodes that help in the agglomeration of micropollutants[16] and to treat wastewater. In our previous work, we treated domestic wastewater of the IIT Mandi campus (collected from the inlet of the Sewage Treatment Plant) by the EC technique that resulted in iron-enriched solid sludge as the byproduct at the end of treatment.[1] Sludge management is usually done by the most common methods of thermal treatment (i.e., calcination), landfilling, and agricultural usage.[17] Wastewater treatment where primary sedimentation is based on the addition of chemicals externally always has a huge chance of a higher content of metal residual in sludge, which may have adverse effects on human health. However, in a few reports, thermal treatment has been applied to convert metal-loaded sludge into a value-added product.[18,19] Electrocoagulated metal-loaded sludge production is one of the big challenges, as its disposal in a landfill is not a sustainable solution. In some cases, sludge waste was used as an ingredient in the formation of a building block[20,21] because it is almost similar to brick clay. But this requires a costly dewatering process. In this work, we found a new method to utilize EC waste as a photoelectrocatalyst without any further treatment. Because of the presence of iron hydroxide in the EC sludge,[22] it is considered an effective photoanode material for water oxidation due to its various properties, i.e., suitable band gap, proper band gap positions, high stability, low cost, and nontoxicity of the material.

2. EXPERIMENTAL SECTION

2.1. Materials and Characterization

Iron (Fe) and aluminum (Al) sheets were used as electrodes for domestic wastewater treatment using the EC technique. The Fe electrode was used as a sacrificial electrode at the anode, and the Fe-enriched hydroxide waste was collected from the top of the EC setup. After centrifugation of flocs by using deionized water as a solvent, settled waste was dried in a hot air oven at 80 °C and utilized directly as an electrocatalyst without any other purification.

The structural characterization of flocs was performed by using X-ray diffraction (PXRD, Philips, The Netherlands) using Cu Kα radiation (λ = 0.154 nm). The microstructure of the samples was analyzed by using field emission scanning electron microscopy (FESEM; Sirion) and transmission electron microscopy (TEM; Tecnai G2 T20 S-TWIN, FEI, Thermo Fisher Scientific) operated at 200 kV. The total surface area was calculated using Brunauer–Emmett–Teller (BET) surface area measurements from a Quantachrome automatic volumetric instrument along with low-pressure volumetric N_2 adsorption measurements with pressure ranging from 0 to 760 Torr. UV–vis diffuse reflectance spectroscopy (DRS) and absorbance spectroscopies were performed with the help of a PerkinElmer UV–vis-near-IR Lambda 750 spectrophotometer using a poly(tetrafluoroethylene) internal reflectance standard. XPS (X-ray photoelectron spectroscopy) of the samples was done using a NEXA instrument with an X-ray source of Al Kα equipped with the Avantage software. Thermogravimetric analysis (TGA) was used to check the stability of the material by using a PerkinElmer instrument with a heating ramp rate of 10 °C/min from room temperature to 800 °C in the presence of air to determine the stability of the electrode.

2.2. Photoelectrochemical Measurements

All electrochemical and photoelectrochemical studies were carried out in a single-compartment three-electrode quartz cell consisting of the working electrode, an Ag/AgCl reference electrode, and a Pt wire counter electrode. The working electrodes were prepared by a drop casting method using catalyst ink on conductive fluorine doped tin oxide (FTO) coated glass substrates. The catalyst ink was prepared by taking 1 mg of the catalyst dispersed in 90 μL of ethanol followed by 10 μL of Nafion solution as a binder and allowed to sonicate for 30 min. Ten microliters of homogeneous ink solution was drop cast on the conducting surface of FTO with an area of 0.5 × 1 cm^2. Thin films coated on FTO were annealed in air at a temperature to attain mechanical stability and to get rid of leaching while measuring in the electrolyte. So, annealing temperature selection is a very critical point; it should not affect the original phase of the material. Hence, TGA was performed to ensure the right selection of the temperature for annealing. The catalyst-modified FTO electrode was further annealed at 400 °C temperature for 30 min with a ramping rate of 10 °C/min in an air atmosphere to improve the adhesion. The material is quite stable up to 400 °C as confirmed with the help of the TGA discussed in a further section. N_2 saturated 0.1 M Na_2SO_4 was utilized as an electrolyte throughout the electrochemical measurements. The current potential polarization (J–V) curves were recorded by using a CHI 608E electrochemical analyzer at a 10 mV/s scan rate. All of the PEC measurements were performed under a 150 W xenon arc lamp (Optosolar GmbH). The electrochemical impedance spectroscopy (EIS) with a sinusoidal perturbation amplitude of 5 mV was recorded at 1.23 V vs RHE within the frequency range of 1 Hz to 1 MHz. The Mott–Schottky analysis was carried out in dark conditions within a potential range of 0 to +1.0 V vs RHE at a frequency of 1 kHz. All experiments were performed using Ag/AgCl as the reference electrode and converting it to RHE (reference hydrogen electrode) by using the Nernst equation given below:

$$E_{RHE} = E_{Ag/AgCl} + 0.059\ pH + 0.19\ V \text{ at } 25\ ^\circ C \quad (1)$$

where 0.19 V is the standard electrode potential of Ag/AgCl (3 M KCl). EC treatment was conducted for different time intervals varying from 20 to 60 min with an interval of 10 min, respectively. The sample coding is denoted as EC_time (min), which means the time used for the EC process; e.g., EC_ 20 min denotes the **E**lectro-**C**oagulation process used for 20 min.

3. RESULTS AND DISCUSSION

Domestic wastewater was treated by using the EC technique in our previous study utilizing Fe and Al as electrodes at the anode and cathode, respectively.[1] In this method, the sacrificial electrode (Fe) gets oxidized and releases (Fe^{x+}; x varies from 2 to 4) cations in the solution. These cations destabilize the suspended particles and pollutants in water through a process called coagulation. The EC process is often used as a wastewater treatment technique as it can facilitate the coagulation and precipitation of contaminants with hydrogen gas as a byproduct at the cathode. The release of hydrogen gas helps in the removal of suspended particles collected at the top of the EC setup.[1] In this work, we are focusing on the waste or sludge generated in this EC process, which usually has the fate of landfill. As sacrificial electrodes (Fe), metal ions are the major constituents in the sludge and are investigated as value-added products for energy production.

https://doi.org/10.1021/acsmaterialsau.4c00006
ACS Mater. Au 2024, 4, 459–467

Scheme 1. EC Setup Used for Wastewater Treatment and Stable Flocs Produced at the Top of the Surface Followed by Drying in the Oven at 80 °C

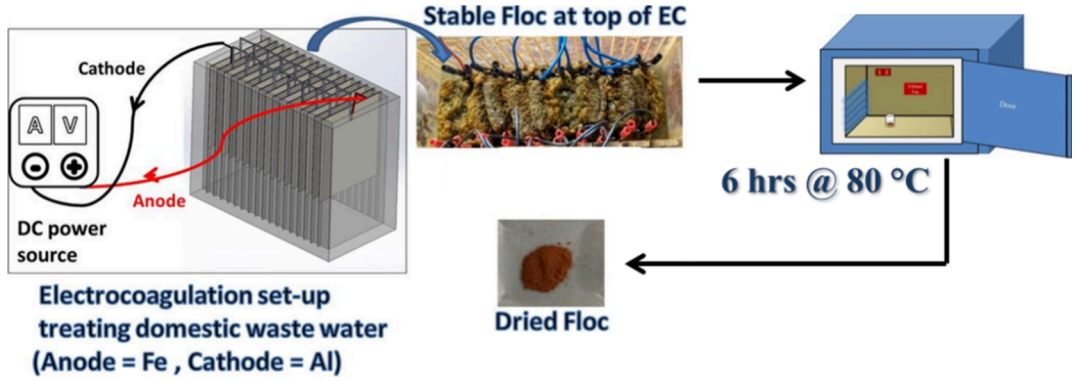

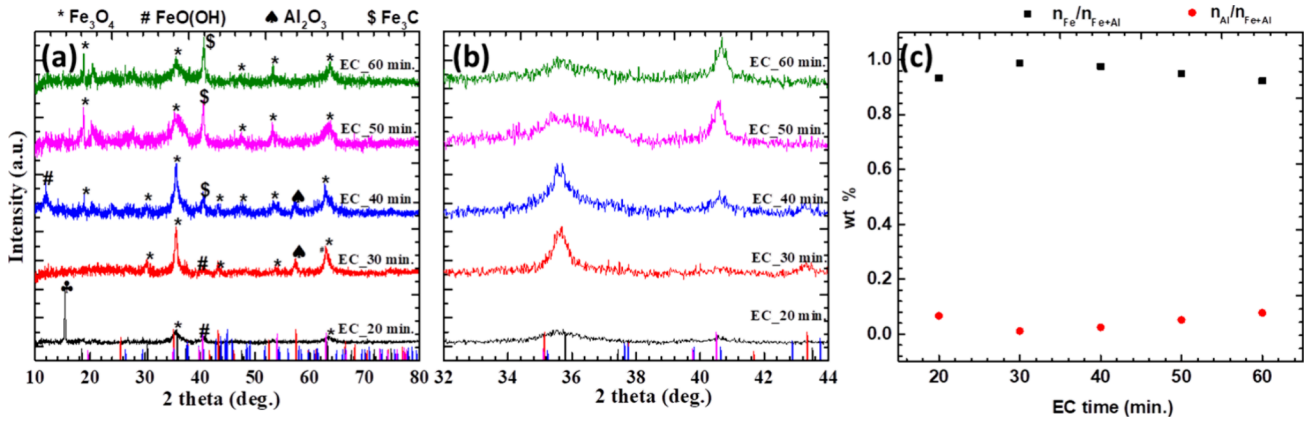

Figure 1. (a) PXRD pattern of flocs obtained after EC treatment time of 20, 30, 40, 50, and 60 min along with the reference patterns of Fe_3O_4 (*Fd*3*m*, 227; black lines), FeOOH (*P*-3*m*1, 164; magenta lines), Al_2O_3 (*R*-3*c*, 167; red lines), and Fe_3C (*Pnma*, 62; blue lines). (b) PXRD in 2θ range from 32 to 44° emphasized more on the evolution of the cementite phase at 40.6°. (c) Metal content quantification by Rietveld refinement.

Stable solid flocs collected at the top of the EC setup surface after treatment as shown in Scheme 1 were collected. The solid flocs were dried in a hot air oven for 6 h at a temperature of 80 °C. The brown-colored solid waste was ground with the help of a mortar pestle and used for further characterization. The composition of the flocs is a function of treatment time that has been varied from 20 to 60 min, denoted as EC_treatment time. PXRD was performed to study the crystallographic information as displayed in Figure. 1a. XRD studies confirmed the formation of the predominant iron oxide (Fe_3O_4) in the magnetite phase with small traces of iron hydroxides (FeOOH). Aluminum oxide (Al_2O_3) was also identified in very small proportions that act as a dopant, present due to the usage of an Al electrode at the cathode. PXRD observation led to the conclusion that the chemical composition of solid waste is largely dependent on the EC treatment time. After 20 min of treatment, aluminum triformate hydrate was formed, which is confirmed by the strong signal observed at 2θ = 15.46 (d = 5.72 Å (002)) as reported in the literature.[23] Meanwhile, flocs collected after 30 min have Fe_3O_4 in the predominant phase confirmed with PXRD peaks observed at 2θ = 18.46, 35.781, 43.50, 47.63, 53.98, and 63.20 corresponding to (111), (113), (004), (133), (224), and (044), respectively (JCPDS pattern of no. 98-007-7592). The Fe electrode as anode acting as the sacrificial electrode provides cations for the electrocoagulation for water treatment, and hence, iron oxide was the major constituent in the floc. However, a very small fraction of aluminum trioxide was also present in the flocs collected on longer treatment of electrocoagulation. The XRD peak at 2θ = 57.48 confirmed the formation of Al_2O_3 in accordance with JCPDS pattern no. 98-000-9770. As EC time increased from 40 to 60 min, the predominant phase formation of iron cementite (Fe_3C: 96.6% of Fe; JCPDS no. 35-0772) along with iron oxide is observed, as shown in Figure 1b. Longer treatment duration increases the iron cementite with simultaneously decreased iron oxide content in the solid flocs mixture. According to EPA report 2013,[24] external supplements of carbon sources brought into wastewater were reported to have a COD (chemical oxygen demand) as high as 1.5 g/L. However, no external carbon source supplements were added during treatment; hence, the C source can be considered as internal, referring to organic carbon substrates present within influent wastewater and endogenous carbon source that are accumulated materials stored within the cells.

The experimental diffraction patterns were subject to a Rietveld refinement to obtain information on the phase purity as well as the phase percentage with the Profex 5.1.1 software package based on the BGMN program.[25] The overall weight % of the metal content along with all refinement parameters is mentioned in Table S1. The Fe content is in maximum proportion at 30 min, with the least Al content that acts as dopant as shown in Figure 1c. As Fe was used as a sacrificial electrode for the treatment of domestic wastewater, flocs collected after treatment were dominated by Fe content and confirmed in the form of iron oxide with a small proportion of Al. Iron-based oxides along with hydroxides (Fe(OOH) have

https://doi.org/10.1021/acsmaterialsau.4c00006
ACS Mater. Au 2024, 4, 459−467

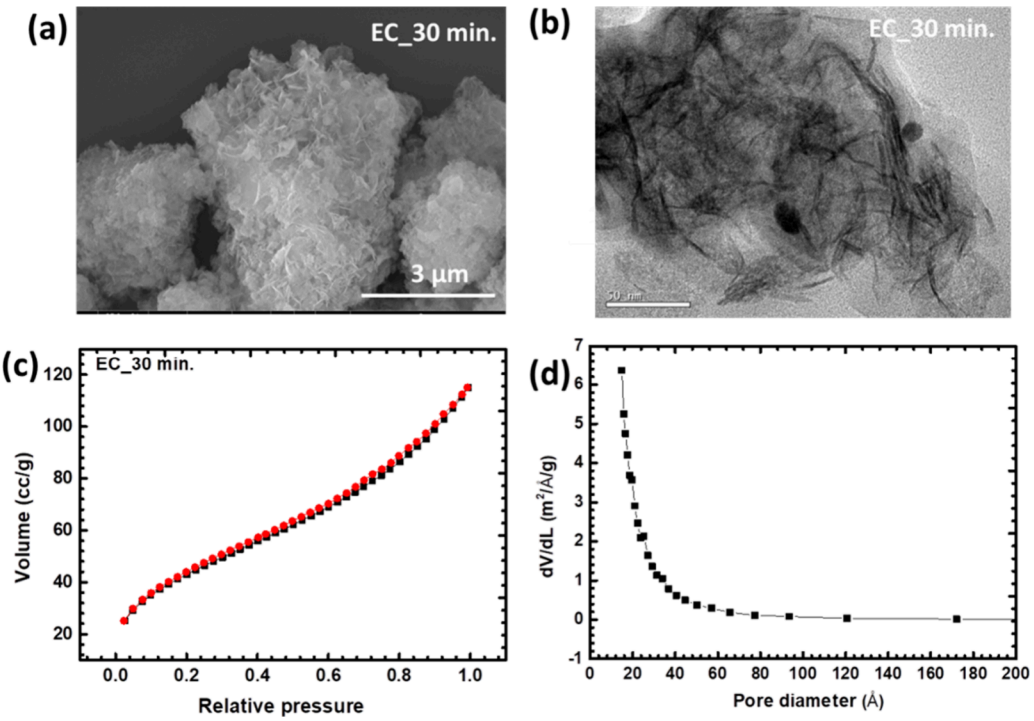

Figure 2. (a) FESEM micrograph, (b) TEM image, (c) BET micrograph, and (d) pore size distribution curve for the EC_30 min sample.

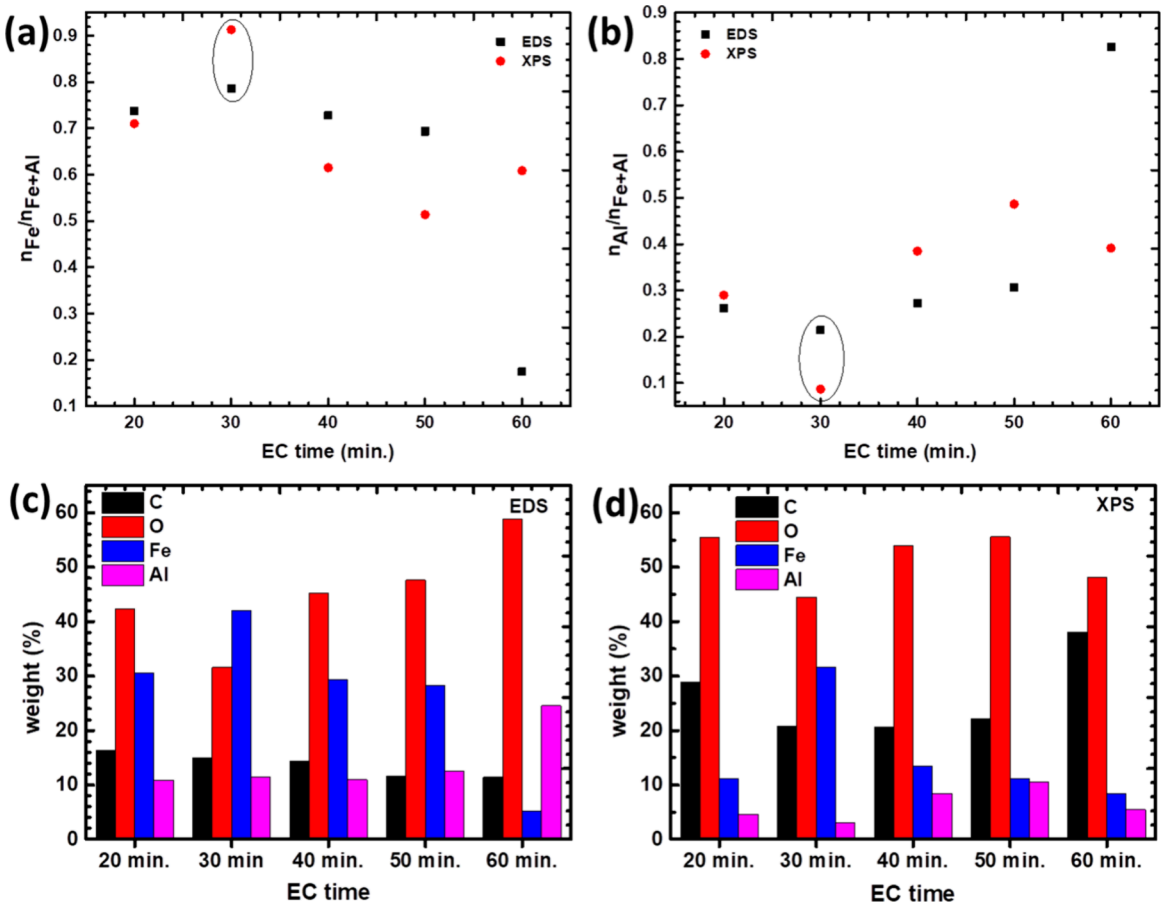

Figure 3. (a) Fe content and (b) Al content w.r.t total metal concentration (Fe and Al) in the catalysts and elemental analysis by the (c) EDAX technique and (d) XPS technique of all samples collected with treatment time of 20, 30, 40, 50, and 60 min, respectively.

https://doi.org/10.1021/acsmaterialsau.4c00006
ACS Mater. Au 2024, 4, 459−467

shown effective activity toward oxygen evolution reaction (OER) due to the low barrier hydrogen bonds.[26] Fe-OOH/(Fe-O_s-H-O) is composed of two different kinds of oxygens where O_s represents oxygen atom bonded to the surface of transition metal oxide, whereas the −OH or hydroxyl group oxygen does not bond to the transition metal and is more facile to open up the hydrogen bond. A hydrogen bond between two O atoms via a center H atom can facilitate such O−H bond breaking when the hydrogen becomes short.[27] Hence, the effect of drying temperature on in situ formed iron hydroxides in the flocs was studied at different temperatures as shown in Figure S1. To confirm the temperature range for drying the flocs without losing iron hydroxides, flocs were dried until the highest selected temperature of 100 °C. FeOOH was stable until 100 °C as confirmed with a characteristic peak at 2θ position of 62.9° and will be very beneficial for water oxidation in sunlight. The strong light absorption capacity of FeOOH can easily generate photogenerated electron pairs.[28] This observation leads to the conclusion of stability of the FeOOH phase until 100 °C. The microstructure of the sample was studied with FESEM, confirming the aggregated form of the nanosheets as shown in Figure 2a for EC_30 min. However, treatment time has no impact on the morphology as confirmed by SEM micrographs as shown in Figure S2 as the treatment time increased from 20 to 60 min. In addition, a small fraction of Al was present in all cases as observed with the help of EDAX (energy-dispersive X-ray analysis) as well as XPS (X-ray photoelectron spectroscopy). Figure 2a shows the SEM micrograph of flocs collected for 30 min. The FESEM micrograph showed aggregated 2D sheet-like structures for 30 min. The increased treatment time leads to more aggregation of nanosheets, as shown in Figure S2. The TEM micrograph also confirmed the 2D nanosheet-like morphology of solid waste after EC in Figure 2b. The adsorption and desorption isotherms of nitrogen gas revealed classic features of iron oxides. The BET-specific surface area of 157.85 $m^2\ g^{-1}$ is reported in the case of EC_30 min and follows a type II isotherm that is mesoporous as shown in Figure 2c. The pore size distribution shown in Figure 2d has confirmed particle size within the range from 20 to 80 Å. The accessible surface area plays a crucial role in the adsorption of the chemical compounds that is appreciable here as the samples were not prepared by any synthesis route and obtained as Fe-enriched waste only.

To check the stability of Fe-enriched floc, TGA was carried out in the presence of air from room temperature to 800 °C as shown in Figure S3. The initial weight loss until 150 °C was due to the adsorbed moisture content present in the flocs, whereas the weight loss observed between 150 and 450 °C was due to the destruction of the labile oxygen functional groups.[29] From 450 to 800 °C, there is almost no change in the weight of the sample, which remains constant. As shown in Figures 3a,b, the EDS as well as XPS analysis is directly giving us confirmation of more Fe-enriched species in all catalysts. In Figures 3a,b, the Fe content is highest in the case of EC_30 in comparison with the least Al content, which coincides with the XRD analysis. The lowest Al concentration in iron oxide shows the relatively best photoelectrochemical performance. However, a higher concentration of Al had a detrimental effect on the photoelectrochemical performance of iron oxide, possibly due to the phase segregation of Al. McFarland et al. have shown by LDA-DFT calculations that an aluminum atom replaces an iron atom in the unit cell and makes very minimal changes to the band edges and remains nondispersive.[30] This suggests that isovalent Al substitution does not make a significant contribution to the electronic structure around the band edges.

The higher photoelectrochemical response with minimal substitution of Al is due to the increase in the conductivity of the material. However, deviation of wt % of Fe and Al in EC_60 in such EDX and XPS may be encountered because of the nonuniformity of sludge at each point. The overall chemical element weight % by both techniques including EDX as well as XPS is shown in Figure 3c,d, respectively. One of the very basic reasons for the variation of the total elemental composition between both techniques is the different penetration or analysis depth that varies from 1 to 3 μm in the case of EDS and 5 to 10 nm in the case of XPS. However, both techniques claimed contaminant-free sludge as no elements other than C, O, Fe, and Al were noticed.

X-ray Photoelectron Spectroscopy (XPS)

The surface analysis was performed by XPS to verify the chemical valences and constituents present in the flocs with different treatment times. The binding energies of the flocs are referred to as the binding energies of the bulk samples obtained by using Al Kα as an X-ray source. High-resolution spectra were analyzed with an analysis spot size of 400 μm with a pass energy of 20 eV. This pass energy corresponds to an Ag $3d_{5/2}$ fwhm of 0.60 eV. Wide scan spectra of XPS performed in a range of 0−1200 eV are shown in Figure S4, which confirmed the presence of Fe, Al, O, and C elements in all samples without any other contamination. The XPS spectrum was fitted with the Avantage software for the core-level spectra for the shape analysis. The peak shape was described by the convolution of the Gaussian−Lorentzian function. Charge neutralization of the samples was analyzed by using the C 1s signal for adventitious carbon. A single peak (Gaussian−Lorentzian) was ascribed to the alkyl type of the carbon (C−C, C−H) obtained at the peak position of 284.8 eV labeled as the main peak of the C 1s spectrum. A second peak at the position of binding energy difference of 1.2 eV is ascribed to alcohols, i.e., C−OH functionalities. In addition, one more peak formed at the higher binding energy, having an energy difference of 3.8 eV corresponding to O−C═O functionalities. In the case of EC_30, the O 1s spectra have special features in comparison to other treatment time samples. Three signals of oxygen were noticed in this case that correspond to three different types of oxygen in the structure as shown in Figure S5 and Table S2. The signal at a binding energy of 529.9 eV ± 0.2 eV corresponds to the signal due to the presence of iron hydroxide,[31] and the signal at a binding energy of 531.3 eV ± 0.2 eV is attributed to oxygen attached to Fe and oxidized Fe at aluminum oxide.[32] The signal at a binding energy of 532.3 eV in case of EC_30 min, corresponds to the adsorbed oxygen, which is absent in other samples.

The high-resolution spectra of Fe 2p for all samples are shown in Figure 4a, which evidenced the existence of Fe^{3+} as well as Fe^{2+} species as tabulated in Table 1. Fe (0) or Fe in the metallic form has a binding energy at the position of 709.8 eV. The absence of such a peak in these samples indicates the absence of any metallic Fe in the species. Core-level spectra of Fe 2p show the Fe^{3+} $2p_{3/2}$ spin−orbit splitting peak at a position of 712 eV. This is also one of the strong evidences for the existence of iron oxide in the form of α Fe_2O_3.[33] The respective shakeup satellite peak should be at a binding energy

https://doi.org/10.1021/acsmaterialsau.4c00006
ACS Mater. Au 2024, 4, 459−467

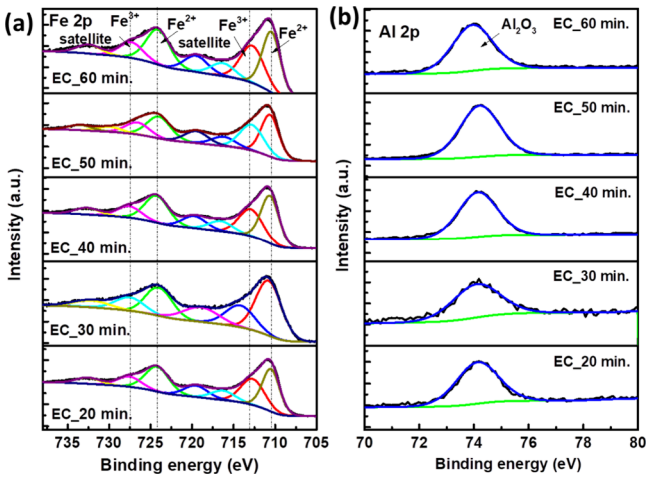

Figure 4. High-resolution XPS spectra of (a) Fe 2p and (b) Al 2p from EC_20 min to EC_60 min samples, respectively.

of 719 eV. However, because of the complexity of the collected waste, it was suspected that the shakeup peak has shifted the position of 716.5 eV, which is still not very clear. Fe $2p_{1/2}$ spin−orbit splitting is observed at a peak position of 724.13 eV, and the respective satellite peak is observed at a position of 8.25 eV ahead of the original peak position. The core-level spectra for iron is for α Fe_2O_3 as the main peak observed for $2p_{3/2}$ has a distinguished signature as compared to γ Fe_2O_3 as described in the literature.[34] A small trace of Al was also present, which is noticed with high-resolution spectra of Al 2p as shown in Figure 4b. In the case of Al 2p spectra, the representative spectrum showed the well-resolved line at 74.2 eV that is assigned to Al 2p spin−orbit components.[35]

Photoelectrochemical performance

The PEC performance of flocs was evaluated by depositing a thin film of catalyst ink suspension on the conducting side of FTO (fluorine-doped tin oxide) and utilizing it as a working electrode. The catalyst coated/FTO was annealed at a temperature of 400 °C with a ramp rate of 10 °C to increase the stability of the thin film over the substrate. PXRD patterns (Figure S6) confirmed that there was no change in the phase of the material after heating.

Mott−Schottky (M−S) analysis was performed as shown in Figure 5 to build an in-depth understanding of the PEC performance of all samples collected at different treatment times. M−S plots were crafted utilizing eq 2:

$$\frac{1}{C_{s^2}} = \frac{2}{N_d A^2 e \in \in_0}\left(V - V_{fb} - \frac{kT}{e}\right) \quad (2)$$

C_s is the space charge layer capacitance, e is the electronic charge, $\in$ is the relative permittivity of the sample, $\in_0$ is the relative permittivity in a vacuum, N_d is the carrier density, KT/e is the temperature-dependent correction term, V is the applied potential, and V_{fb} is the flat band potential. The plot of A^2/C_s^2 vs V is referred to as a typical M−S plot, and extrapolation to the horizontal axis gives the flat band potential of the electrode materials. A clear positive slope depicts the n-type behavior of the semiconductor with electrons as the majority carrier.[36] There is a correlation between the cathodic shift in V_{fb} and the onset potential of waste-derived samples. The highest cathodic shift was observed in the case of EC_30 min with V_{fb} of 0.39 V in comparison to 0.49 V (EC_20 min), 0.51 V (EC_40 min), 0.49 V (EC_50 min), and 0.41 V (EC_60 min), respectively. Such cathodic shift in V_{fb} was favorable for electrons to pass through the circuit to counter electrode that results in a decrease in onset potential for anodic reaction that is helpful for improved photoelectrochemical performance.

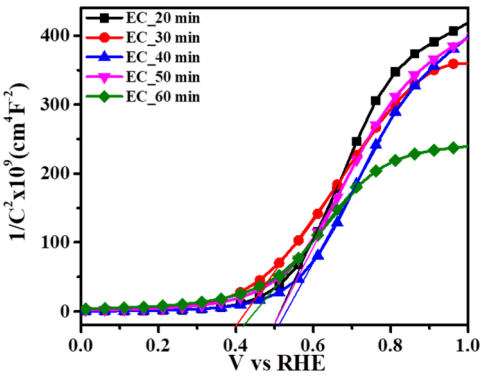

Figure 5. Mott−Schottky plot of solid flocs after varying the EC treatment time in 0.1 M Na_2SO_4.

The PEC experiments were performed in a standard three-electrode configuration in 0.1 M Na_2SO_4 solution under standard illumination of AM 1.5 G. Figure 6a shows the photocurrent density−potential (J−V) curves under dark and light illumination for flocs collected with different treatment times. The PEC properties were examined by considering the two prominent features: one is the saturated photocurrent density observed at the thermodynamic potential of water oxidation reaction (1.23 V), and another is the onset potential for photocurrent. Among the all studied samples, EC_30 min has the highest photocurrent density and a cathodic shift in onset potential. The photocurrent density of EC_30 min was reported to be 4.6×10^{-6} A cm^{-2} under light illumination at a potential of 1.23 V vs RHE. After 30 min, a decrement in the current density can be correlated to the increment in the Al content as determined by Rietveld refinement. A higher concentration of Al has a detrimental effect on the PEC performance of iron oxide based photoanode due to the segregation of Al. McFarland et al. reported[30] the positive effect of Al doping in iron-based oxides at a certain level of

Table 1. Binding Energy Illustration of Fe 2p Spectra

sample Fe 2p	Fe $^{2+}$ $2p_{3/2}$	ΔE (sat. Fe $^{2+}$ $2p_{3/2}$)	Fe $^{2+}$ $2p_{1/2}$	ΔE (sat. Fe $^{2+}$ $2p_{3/2}$)	Fe $^{3+}$ $2p_{3/2}$	Fe $^{3+}$ $2p_{1/2}$	shake-up satellite peak
	eV	eV	eV	eV	eV	eV	eV
EC_20 min	710.57	9.17	724.55	8.13	712.98	727.65	716.52
EC_30 min	710.8	8.19	724.13	8.25	714.46	727.76	
EC_40 min	710.68	9.05	724.55	8.47	713.09	727.52	716.65
EC_50 min	710.68	9.06	724.21	9.39	712.98	726.61	716.30
EC_60 min	710.57	9.16	724.32	8.36	712.86	727.56	716.41

https://doi.org/10.1021/acsmaterialsau.4c00006
ACS Mater. Au 2024, 4, 459−467

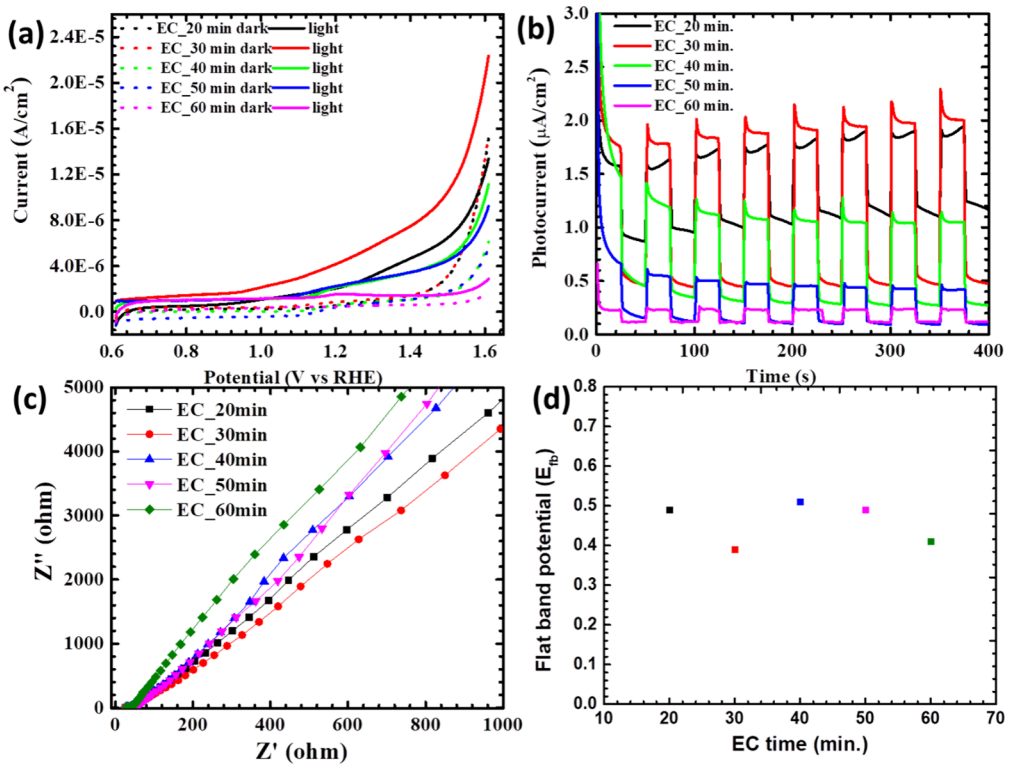

Figure 6. (a) Photocurrent density−voltage curve of flocs (dotted lines for dark conditions and solid lines in the presence of light). (b) Transient photocurrent curves with on−off cycles. (c) Nyquist plot. (d) Flat band potential derived from the Mott−Schottky plot for EC_20 min to EC_60 min samples in 0.1 M Na_2SO_4 electrolyte.

substitution where Fe^{3+} got replaced by Al^{3+}, benefiting small polaron migration and resulting in the improvement in conductivity in comparison to the Al-rich samples. However, a higher content of Al segregates at the grain boundaries, and as a result, photocurrent density also diminished. However, photocurrent density remained as a function of potential, with a higher current density with high external biasing at the interface. The presence of the hydroxide intermediate at the interface leads to the formation of the *OOH intermediate readily, which determines the rate of the reaction. Hence, in the case of the EC_30 min sample, the rate of reaction was expected to be higher with low overvoltage due to the presence of hydroxides resulting in a high rate of reaction.

Transient photocurrent density with chopped light having 25 s on and 25 s off cycles was also studied for all samples, as shown in Figure 6b. EC_30 min shows the highest photocurrent density with on−off cycles that is due to the fast response and recovery time. The positive spikes in the photocurrent correspond to the accumulation of the holes in the electrode space charge layer under illumination. The observed stable photocurrent corresponds to the charge carrier concentration in the space charge layer. And the highest photocurrent directly gives a hint of the maximum charge carrier density supporting the results of characteristic $J-V$ curves. The interfacial charge transfer resistance was studied with the help of electrochemical impedance spectroscopy (EIS). The Nyquist plot as shown in Figure 6c has been obtained at a potential of 1.23 V in the frequency range from 1 to 10 M Hz, respectively. All samples have the same solution resistance which was attributed to the ions present in the solution or electrolyte and called solution resistance (R_s).

As we move from the higher-frequency region to the lower-frequency region, the interfacial charge transfer resistance (R_{ct}) contributes, which is less in the case of the EC_30 min sample in comparison to the rest of the samples, indicating facile charge transfer kinetics at the interface. EIS and M−S analyses show that EC_30 min exhibits the lowest charge transfer resistance and cathodic shift in V_{fb}, respectively, and concludes the fast electron transfer at the interface with low onset potential in the case of anodic photocurrent.

The total cost of operation (TCO) is the result of the sum of different costs associated with EC process operation, as indicated by eq 3:

$$\begin{aligned} \mathrm{TCO} = {} & (\text{electricity price} \times \text{energy consumption} \\ & + \text{anode price} \times \text{electrode consumption}) \\ & + \text{sludge disposal cost} \times \text{sludge generate} \end{aligned} \tag{3}$$

The TCO equation can be divided into two parts: one is the electricity and electrode consumption during EC, and the other is sludge management. In WWTPs, disposal and treatment of the sewage sludge account for 40−50% of the total operating cost.[37] Landfilling, agricultural usage, and thermal treatment are the most common ways opted for sludge treatment.[17] The electricity consumption in the case of the EC process was calculated as 0.017 kWh operated at 1.25 mA cm^{-2} in our previous report.[1] The electrode consumed during the process was recovered as a value-added product. Hence, this way of waste water treatment along with sludge recovery is a very cost-effective and sustainable technique. And the main contributing part toward electricity consumption includes electrocoagulation process and drying of the sludge. Considering that a hot air oven operates at 220 V and the heating

https://doi.org/10.1021/acsmaterialsau.4c00006
ACS Mater. Au 2024, 4, 459−467

element draws a current of 10 A, the power of the heating element can be calculated as the product of volts × current, resulting in 2200 W. An oven utilizing full power for 6 h means 13.2 kWh; however, the element is usually controlled by a thermostat that maintains the target temperature. The temperature is quite low here, 80 °C, which means even less consumption of electricity in total. Hence, the zero-based approach of wastewater treatment through electrocoagulation is a very cost-effective process.

This work shows photocatalyst recovery from electrocoagulation waste collected after the treatment of domestic wastewater. The EC technique is associated with large operation costs, and excess floc formation appears to be a serious drawback in the existing EC processes. The waste generated by the EC process can be used as a photoelectrode due to the presence of iron oxide and (oxygen) hydroxides. The presence of FeOOH makes this wasted floc an effective catalyst as FeOOH is composed of a metal oxy-hydroxyl bond, which might have a short $O_s\cdots H-O_{ad}$ (O_s represents oxygen atoms bonded to the surface of the transition metal oxide, whereas O_{ad} represents hydroxyl groups or oxygen atoms of nonbonded water molecules that are not bonded to transition metals). This helps to open the hydrogen bond of water and thus escalates the water oxidation. Thus, the catalytic activity of the water oxidation process depends upon the availability of the surface-active species and OER active surface sites.[20] In our experimental data, the EC_30 min sample, which reported the highest amount of Fe content with minimal Al doping and which acts as a dopant, has the highest water oxidation activity, indicating that FeOOH is the activity descriptor for this water oxidation process.

4. CONCLUSIONS

In this study, we have collected the waste produced after the treatment of domestic wastewater by using the EC technique, where Fe (sacrificial electrodes, anode) and Al (cathode) were used. Phase studies of waste were characterized with the help of PXRD and found to be in the magnetite form. Microstructural characterization (TEM) confirmed that waste exists in a agglomerated 2D nanosheet-like morphology with the highest iron hydroxide content present in the sample treated for 30 min. The samples were deposited over the FTO surface and studied for PEC water oxidation under standard illumination of AM 1.5 G. The sample with the highest content of Fe along with minimal Al content that acts as a dopant shows the best performance in terms of a photocurrent density of 4.6×10^{-6} A cm^{-2} at a potential of 1.23 V. EIS and Mott−Schottky analysis studies revealed low charge transfer resistance, revealing less obstruction in the charge flow at the interface with a lower onset potential in comparison to the other samples.

ASSOCIATED CONTENT

Supporting Information

The Supporting Information is available free of charge at https://pubs.acs.org/doi/10.1021/acsmaterialsau.4c00006.

PXRD of EC_30 min at different drying temperatures; Rietveld refinement details; FESEM images, thermogravimetric analysis (TGA) of EC_30 min; XPS survey spectrum; high-resolution XPS spectra of C 1s and O 1s with full details; and PXRD of FTO and FTO/flocs at 400 °C (PDF)

AUTHOR INFORMATION

Corresponding Author

Aditi Halder − *School of Chemical Sciences, Indian Institute of Technology Mandi, Kamand 175005, India;* orcid.org/0000-0003-0399-9705; Email: aditi@iitmandi.ac.in

Authors

Lalita Sharma − *School of Chemical Sciences, Indian Institute of Technology Mandi, Kamand 175005, India;* orcid.org/0000-0002-1924-3913

Jyoti Rohilla − *Department of Chemistry, Indian Institute of Technology Delhi, New Delhi 110016, India*

Pravin P. Ingole − *Department of Chemistry, Indian Institute of Technology Delhi, New Delhi 110016, India;* orcid.org/0000-0002-9755-4477

Complete contact information is available at: https://pubs.acs.org/10.1021/acsmaterialsau.4c00006

Author Contributions

CRediT: **Lalita Sharma** conceptualization, data curation, formal analysis, investigation, writing-original draft, writing-review & editing; **Jyoti Rohilla** data curation, formal analysis; **Pravin Popinand Ingole** formal analysis, supervision, validation, writing-review & editing; **Aditi Halder** conceptualization, funding acquisition, project administration, supervision, writing-review & editing.

Notes

The authors declare no competing financial interest.

ACKNOWLEDGMENTS

The authors want to acknowledge AMRC, IIT Mandi, for providing instrument facilities and MHRD, India, for the financial support.

REFERENCES

(1) Sharma, L.; Prabhakar, S.; Tiwari, V.; Dhar, A.; Halder, A. Optimization of EC parameters using Fe and Al electrodes for hydrogen production and wastewater treatment. *Environmental Advances* **2021**, *3*, No. 100029.

(2) Tsakiridis, P. E. Aluminium salt slag characterization and utilization − A review. *Journal of Hazardous Materials* **2012**, *217*−*218*, 1−10.

(3) Blankenship, R. E.; Tiede, D. M.; Barber, J.; Brudvig, G. W.; Fleming, G.; Ghirardi, M.; Gunner, M. R.; Junge, W.; Kramer, D. M.; Melis, A.; Moore, T. A.; Moser, C. C.; Nocera, D. G.; Nozik, A. J.; Ort, D. R.; Parson, W. W.; Prince, R. C.; Sayre, R. T. Comparing photosynthetic and photovoltaic efficiencies and recognizing the potential for improvement. *Science* **2011**, *332* (6031), 805−809.

(4) Luo, J.; Vermaas, D. A.; Bi, D.; Hagfeldt, A.; Smith, W. A.; Grätzel, M. Bipolar membrane-assisted solar water splitting in optimal pH. *Adv. Energy Mater.* **2016**, *6* (13), No. 1600100.

(5) Roger, I.; Shipman, M. A.; Symes, M. D. Earth-abundant catalysts for electrochemical and photoelectrochemical water splitting. *Nat. Rev. Chem.* **2017**, *1* (1), 1−13.

(6) McCrory, C. C.; Jung, S.; Ferrer, I. M.; Chatman, S. M.; Peters, J. C.; Jaramillo, T. F. Benchmarking hydrogen evolving reaction and oxygen evolving reaction electrocatalysts for solar water splitting devices. *J. Am. Chem. Soc.* **2015**, *137* (13), 4347−4357.

(7) Pu, Z.; Liu, Q.; Jiang, P.; Asiri, A. M.; Obaid, A. Y.; Sun, X. CoP nanosheet arrays supported on a Ti plate: an efficient cathode for electrochemical hydrogen evolution. *Chem. Mater.* **2014**, *26* (15), 4326−4329.

(8) Gerken, J. B.; Shaner, S. E.; Massé, R. C.; Porubsky, N. J.; Stahl, S. S. A survey of diverse earth abundant oxygen evolution

electrocatalysts showing enhanced activity from Ni−Fe oxides containing a third metal. *Energy Environ. Sci.* **2014**, *7* (7), 2376−2382.
(9) Gong, M.; Li, Y.; Wang, H.; Liang, Y.; Wu, J. Z.; Zhou, J.; Wang, J.; Regier, T.; Wei, F.; Dai, H. An advanced Ni−Fe layered double hydroxide electrocatalyst for water oxidation. *J. Am. Chem. Soc.* **2013**, *135* (23), 8452−8455.
(10) Sun, J.; Sun, L.; Yang, X.; Bai, S.; Luo, R.; Li, D.; Chen, A. Photoanode of coupling semiconductor heterojunction and catalyst for solar PEC water splitting. *Electrochim. Acta* **2020**, *331*, No. 135282.
(11) Rangaraju, R.; Panday, A.; Raja, K.; Misra, M. Nanostructured anodic iron oxide film as photoanode for water oxidation. *J. Phys. D: Appl. Phys.* **2009**, *42* (13), No. 135303.
(12) Cao, X.; Xu, C.; Liang, X.; Ma, J.; Yue, M.; Ding, Y. Rationally designed/assembled hybrid BiVO4-based photoanode for enhanced photoelectrochemical performance. *Applied Catalysis B: Environmental* **2020**, *260*, No. 118136.
(13) Zhang, X.; Zhang, B.; Luo, Y.; Lv, X.; Shen, Y. Phosphate modified N/Si co-doped rutile TiO2 nanorods for photoelectrochemical water oxidation. *Appl. Surf. Sci.* **2017**, *391*, 288−294.
(14) Holt, P. K.; Barton, G. W.; Mitchell, C. A. The future for electrocoagulation as a localised water treatment technology. *Chemosphere* **2005**, *59* (3), 355−367.
(15) Chen, G. Electrochemical technologies in wastewater treatment. *Sep. Purif. Technol.* **2004**, *38* (1), 11−41.
(16) Pan, C.; Troyer, L. D.; Catalano, J. G.; Giammar, D. E. Dynamics of chromium (VI) removal from drinking water by iron electrocoagulation. *Environ. Sci. Technol.* **2016**, *50* (24), 13502−13510.
(17) Diamantis, V.; Erguder, T. H.; Aivasidis, A.; Verstraete, W.; Voudrias, E. Wastewater disposal to landfill-sites: A synergistic solution for centralized management of olive mill wastewater and enhanced production of landfill gas. *Journal of Environmental Management* **2013**, *128*, 427−434.
(18) Thabet, R. H.; Fouad, M. K.; Sherbiny, S. A. E.; Tony, M. A. Zero-waste approach: assessment of aluminum-based waste as a photocatalyst for industrial wastewater treatment ecology. *Int. J. Environ. Res.* **2022**, *16* (3), 36.
(19) Zhao, Y.-x.; Li, X.-y.; Tian, C.; Wang, J.-x. Production of carbon-doped titanium dioxide (C−TiO2) from polytitanium-coagulated sludge as an adsorbent or photocatalyst for pollutant removals. *Journal of Cleaner Production* **2020**, *267*, No. 121979.
(20) Adyel, T. M.; Rahman, S. H.; Zaman, M. M.; Sayem, H. M.; Khan, M.; Abdul Gafur, M.; Islam, S. M. N. Reuse Feasibility of Electrocoagulated Metal Hydroxide Sludge of Textile Industry in the Manufacturing of Building Blocks. *J. Waste Manag.* **2013**, *2013*, No. 686981.
(21) Amsayazhi, P.; Saravana Raja Mohan, K. Use of sludge waste as ingredient in making of brick. *Int. J. Eng. Technol.* **2018**, *7*, 419−422.
(22) Sharma, P.; Jang, J. W.; Lee, J. S. Key strategies to advance the photoelectrochemical water splitting performance of α-Fe2O3 photoanode. *ChemCatChem.* **2019**, *11* (1), 157−179.
(23) Väänänen, M.; Kupiainen, L.; Rämö, J.; Sarpola, A.; Tanskanen, J. Speciation and coagulation performance of novel coagulant − Aluminium formate. *Sep. Purif. Technol.* **2012**, *86*, 242−247.
(24) Fact, E. W. T. *Sheet: External Carbon Sources for Nitrogen Removal*; Environmental Protection Agency Office of Wastewater Management: Washington, DC, USA,2013.
(25) Shannon, R. D. Revised effective ionic radii and systematic studies of interatomic distances in halides and chalcogenides. *Acta crystallographica section A: crystal physics, diffraction, theoretical and general crystallography* **1976**, *32* (5), 751−767.
(26) Cleland, W. W., The low-barrier hydrogen bond in enzymic catalysis. In *Adv. Phys. Org. Chem.*, Richard, J. P.; Ed. Academic Press: 2010; Vol. *44*, pp 1−17.
(27) Yang, J.; Zheng, J.; Xu, M.; Zhuo, Z.; Yang, W.; Wang, L.-W.; Dai, L.; Lu, J.; Amine, K.; Pan, F. Short hydrogen bonds on reconstructed nanocrystal surface enhance oxygen evolution activity. *ACS Catal.* **2018**, *8* (1), 466−473.
(28) Weng, H.; Yang, Y.; Zhang, C.; Cheng, M.; Wang, W.; Song, B.; Luo, H.; Qin, D.; Huang, C.; Qin, F.; Li, K. Insight into FeOOH-mediated advanced oxidation processes for the treatment of organic polluted wastewater. *Chemical Engineering Journal* **2023**, *453*, No. 139812.
(29) Liang, Y.; Lu, W. Gamma-irradiation synthesis of Fe3O4/rGO nanocomposites as lithium-ion battery anodes. *Journal of Materials Science: Materials in Electronics* **2020**, *31* (19), 17075−17083.
(30) Kleiman-Shwarsctein, A.; Huda, M. N.; Walsh, A.; Yan, Y.; Stucky, G. D.; Hu, Y.-S.; Al-Jassim, M. M.; McFarland, E. W. Electrodeposited aluminum-doped α-Fe2O3 photoelectrodes: experiment and theory. *Chem. Mater.* **2010**, *22* (2), 510−517.
(31) Allen, G. C.; Curtis, M. T.; Hooper, A. J.; Tucker, P. M. X-Ray photoelectron spectroscopy of iron−oxygen systems. *J. Chem. Soc., Dalton Trans.* **1974**, *14*, 1525−1530.
(32) Paparazzo, E. XPS and auger spectroscopy studies on mixtures of the oxides SiO2, Al2O3, Fe2O3 and Cr2O3. *J. Electron Spectrosc. Relat. Phenom.* **1987**, *43* (2), 97−112.
(33) Xu, L.; Xia, J.; Wang, L.; Qian, J.; Li, H.; Wang, K.; Sun, K.; He, M. a-Fe2O3 cubes with high visible-light-activated photoelectrochemical activity towards glucose: hydrothermal synthesis assisted by a hydrophobic ionic liquid. *Chemistry* **2014**, *20*, 2244−2253.
(34) McIntyre, N. S.; Zetaruk, D. G. X-ray photoelectron spectroscopic studies of iron oxides. *Anal. Chem.* **1977**, *49* (11), 1521−1529.
(35) Yang, C.-S.; Kim, J.-S.; Choi, J.-W.; Kwon, M.-H.; Kim, Y.-J.; Choi, J.-G.; Kim, G.-T. XPS study of aluminum oxides deposited on PET thin film XPS study of aluminum oxides deposited on PET thin film. *J. Ind. Eng. Chem.* **2000**, *6* (3), 149−156.
(36) Dey, K. K.; Gahlawat, S.; Ingole, P. P. BiVO 4 optimized to nano-worm morphology for enhanced activity towards photo-electrochemical water splitting. *Journal of Materials Chemistry A* **2019**, *7* (37), 21207−21221.
(37) Chi, Y.; Tian, C.; Li, H.; Zhao, Y. Polymerized Titanium Salts for Algae-Laden Surface Water Treatment and the Algae-Rich Sludge Recycle toward Chromium and Phenol Degradation from Aqueous Solution. *ACS Sustainable Chem. Eng.* **2019**, *7* (15), 12964−12972.

https://doi.org/10.1021/acsmaterialsau.4c00006
ACS Mater. Au 2024, 4, 459−467